IEEE Access
Multidisciplinary | Rapid Review | Open Access Journal

Received February 10, 2021, accepted April 5, 2021, date of publication April 9, 2021, date of current version April 19, 2021.

Digital Object Identifier 10.1109/ACCESS.2021.3072054

Belt-Driven Integrated Starter and Generator Using Planetary Gears for Micro Hybrid Electric Vehicles

SEONWOO JEON[1], GANG SEOK LEE[1], DONG-WOO KANG[2], (Member, IEEE), WON-HO KIM[3], AND SUNGWOO BAE[1], (Member, IEEE)

[1]Department of Electrical Engineering, Hanyang University, Seoul 04763, South Korea
[2]Department of Electrical Engineering, Keimyung University, Daegu 42601, South Korea
[3]Department of Electrical Engineering, Gachon University, Seongnam 13120, South Korea

Corresponding author: Sungwoo Bae (swbae@hanyang.ac.kr)

This work was supported by the Technology Innovation Program (20002777, Development of energy harvesting for automotive auxiliary power system APN and technology utilization) funded By the Ministry of Trade, Industry & Energy (MOTIE, Korea).

ABSTRACT This paper presents a 12 V mechanical torque converting belt-driven integrated starter and generator (BSG) system without a DC-DC converter. A micro hybrid electric vehicle (micro HEV) typically uses a 12 V battery with a 12/48 V bidirectional DC-DC converter to satisfy its high starting torque and wide operating speed for generating the required power. In contrast, the proposed BSG consists of a wound field synchronous machine (WFSM), planetary gears, and a belt-type pulley, which does not require an additional bidirectional DC-DC converter. Owing to the mechanical torque converter, the proposed BSG system produces a high starting torque in starter-mode with a 12:1 gear ratio, and it operates in generator-mode with a 1:2 gear ratio to satisfy the required target specifications. To verify that the proposed BSG system meets the required target design specifications, simulations using MATLAB/Simulink 2018b and ANSYS electromagnetic 19.0 were performed. Additionally, the experimental results verify that this proposed BSG meets the required starter and generator modes specifications. Based on an analysis of the cost and vehicle environment conditions, the proposed BSG provides an efficient solution to the high cost issue incurred by a micro-HEV that requires a DC-DC converter system.

INDEX TERMS Belt-driven starter and generator, field-current control, mechanical torque converter, micro hybrid electric vehicles, wound field synchronous machine.

I. INTRODUCTION

A. RELATED WORK AND MOTIVATION

Owing to the increased fuel efficiency regulations required of automobile manufacturers and the increased demand for high fuel economy from consumers, hybrid electric vehicles (HEVs) has been developed [1]–[3]. These HEVs are classified as micro HEVs, mild HEVs, and full HEVs depending on the operating voltage and electrical power level. Among these HEVs, this study focuses on micro HEVs that use a 12 V battery, because the need for these micro-HEVs has steadily increased in the market [3].

The first-generation micro-HEV employs a 12 V battery system that uses an enhanced starter motor with a separate alternator to implement an idle stop-and-go function, as presented in TABLE 1. The second-generation micro-HEV, powered by a 12 V battery, uses a belt-driven integrated starter and generator (BSG) [4], [5]. As presented in TABLE 1, this boost-type BSG micro HEV offers an improved fuel economy with a voltage-boosting system such as an additional DC-DC converter. This is because the size of the 12 V battery powered BSG can be increased to produce the torque required in starter-mode. In other words, a high current is required by starter-mode operation of a 12 V BSG system [6], [7]. Therefore, to resolve the design and high current issues of the BSG, this boost-type BSG typically requires an additional DC-DC converter to step up the 12 V battery voltage to the BSG operating voltage (i.e., 48 V) [8].

This boost-type BSG micro HEV entails an additional manufacturing cost because of the required additional

The associate editor coordinating the review of this manuscript and approving it for publication was Guangya Yang.

TABLE 1. Comparison of micro HEVs powered by a 12 V battery.

Micro HEV type	1st-generation micro HEV	Boost-type BSG micro HEV	Proposed BSG micro HEV
Structure	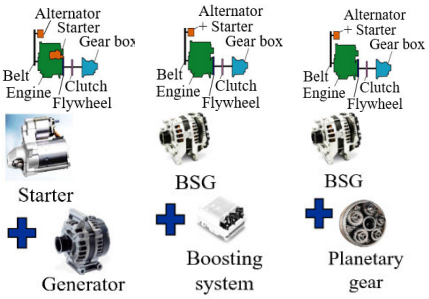		
Boost type	None	DC-DC converter	Mechanical torque converter
Fuel economy improvement	3%	4%–5%	4%–5%
Cost	Low	High	Intermediate
System complexity	Low	High	Intermediate

DC-DC converter. As presented in TABLE 1, the manufacturing cost of this boost-type BSG micro-HEV system is higher than that of the first-generation micro-HEV system according to the original automotive equipment manufacturer [4]–[8]. The boosting power conversion stage also requires additional mounting space and many electronic components, including a controller, resulting in increased complexity of the overall system [4]–[8]. In addition, complete insulation between 12 V and 48 V is required for the protection and safety of electronic components in the vehicle.

In addition, a BSG micro HEV requires a wide operating range of power generation under various load conditions to improve the fuel efficiency and charge the battery. When a DC motor is used for a micro HEV BSG system, there is a limitation on the wide operating range due to the limitation of the stator voltage during high-speed operation [9]. Achieving a wide power generation range under various load conditions requires field-weakening control at high speed [10], [11]. In addition, to satisfy the voltage limitation in high-speed operation, parameters such as the stator, rotor, and windings should be considered [10], [11].

To resolve these issues, a wound field synchronous machine (WFSM) with a mechanical torque converter for a 12 V BSG micro-HEV (see TABLE 1) is proposed. When this WFSM is used as a BSG, operation at high speed under field-weakening control is possible. It also has a high power factor and a wide operating range in power generation, which are important for the BSG function [12], [13]. This WFSM with a mechanical torque converter has different gear ratios in accordance with the clockwise (CW) direction in the starter-mode and the counterclockwise (CCW) direction in generator-mode. As a result of the high gear ratio in starter-mode of the proposed BSG system, the 12 V BSG with a mechanical torque converter can achieve the required high starting torque. In other words, the proposed BSG system that uses a pulley, planetary gears, and a 12 V BSG can produce a high torque without a DC-DC converter. Hence, if this mechanical torque converter is applied, the BSG and the entire control system can be simplified. For detecting the defects of this mechanical torque converter, vibration-based techniques can be used, which are widely used as methods for diagnosing defects in planetary gears [14], [15]. As given in TABLE 1, its production cost can be reduced in comparison with that of the voltage-boosting-type BSG system. Additionally, the proposed WFSM for a 12 V BSG micro-HEV uses a field-weakening control to satisfy a wide power generation range under various load conditions [16], [17]. Because the proposed WFSM BSG system controls the field current with Hall sensors, it is possible to simplify the control method and reduce the cost of the control system [18], [19]. Therefore, the proposed WFSM with a mechanical torque converter is particularly useful for a BSG system requiring a high torque in starter-mode and a wide power generation range.

B. PAPER CONTRIBUTION

The main contributions of this study are summarized as follows:

- Solution for the unit cost issue of the boost-type BSG system: By replacing the various electronic components that make up the boosting system with a structurally simple mechanical torque converter, the proposed 12 V BSG system results in a more cost-effective solution.
- Analysis of electrical and mechanical effects of the 12 V BSG according to component temperature variation: By comparing variations in electrical characteristics of power semiconductors and variations in mechanical characteristics of the mechanical torque converter, it was derived that the proposed mechanical torque converter has a lower influence at high temperature.
- Suggestion of suitable 12 V BSG motor type selection method: Through the proposed algorithm for satisfying required characteristics, it can be confirmed which motor type (PMSM, WFSM) is suitable for the 12 V BSG before design.
- Performance verification of the proposed 12 V WFSM BSG with a mechanical torque converter system: The proposed 12 V WFSM BSG with a mechanical torque converter was shown to exhibit the required starting torque and a wide power generation range under various load conditions for a 12V micro-HEV through simulation and experimental analysis.

C. PAPER STRUCTURE

To demonstrate this 12 V BSG system, the remainder of this paper is organized as follows. Section II presents an electrical and mechanical effects comparison of a bidirectional DC-DC converter and the mechanical torque converter according to temperature variation. In addition, through the proposed algorithm, which motor type (PMSM, WFSM) is suitable

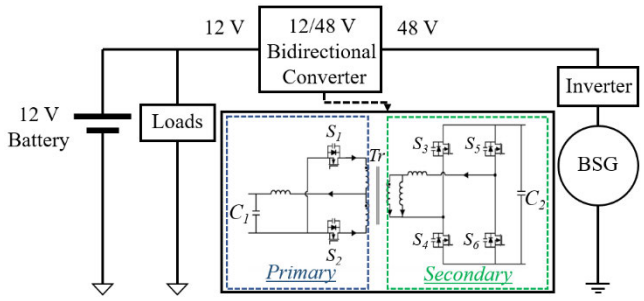

FIGURE 1. Boost-type BSG using a 12/48 V bidirectional DC-DC converter.

TABLE 2. Parameters of the 12/48 V bidirectional DC-DC converter.

Parameter name	Value	Unit
Primary voltage range	10~16	[V]
Secondary voltage range	40~52	[V]
Maximum output power	1.8	[kW]
Switching frequency	100	[kHz]
Output current ripple	10	[%]
Output voltage ripple	10	[%]
Transformer turn ratio	4:2:2	N/A
Filter inductance	6	[uH]
Filter capacitance	13.2	[uF]
Secondary capacitance	10	[uF]

for the 12 V BSG system is presented. Section III describes the simulation studies of starter and generator modes with MATLAB/Simulink and ANSYS electromagnetic 19.0 to verify the bidirectional control algorithm for the proposed WFSM BSG with target specifications. Section IV presents experimental results that demonstrate the performance of the proposed WFSM BSG system; the results demonstrate that this WFSM BSG system is suitable for a 12 V micro HEV BSG system. Finally, Section V concludes this paper with summaries and findings.

II. 12 V WFSM BSG WITH A MECHANICAL TORQUE CONVERTER

A. COMPARISON OF A 12/48 V BIDIRECTIONAL DC-DC CONVERTER AND MECHANICAL TORQUE CONVERTER

In this section, the operating characteristics and cost of between a 12/48 V bidirectional DC-DC converter and the proposed mechanical torque converter are compared. First, the schematic of the 12/48 V bidirectional DC-DC converter type BSG is shown in Fig. 1, and the 12/48 V bidirectional DC-DC converter parameters are presented in TABLE 2. In starter-mode, the bidirectional DC-DC converter operates in boost-mode. In generator-mode, the bidirectional DC-DC converter operates in buck-mode for battery charging. The 12/48 V bidirectional DC-DC converter applied to a micro-HEV generally uses a full-bridge/push-pull structure [20]. Therefore, a full-bridge/push-pull structure of the 12/48 V bidirectional DC-DC converter was analyzed in this section. In buck-mode, phase shifted pulse width modulation

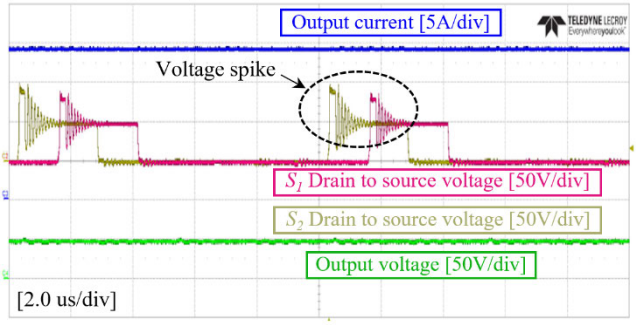

FIGURE 2. Switch voltage spikes of the manufactured bidirectional DC-DC converter in boost-mode.

is implemented with zero-voltage-switching (ZVS). However, the 12/48 V bidirectional DC-DC converter has high voltage spikes of switches (S_1, S_2) in boost-mode as shown in Fig. 2. These high voltage spike of switches (S_1, S_2) may cause severe damage in the power conversion operation. As a solution to the high voltage spike of switches (S_1, S_2), a snubber circuit using resistors and capacitors or the active clamping method with additional switches is employed [21], [22]. Although these methods can solve the high voltage spike of switches, they reduce the efficiency and increase the volume and cost.

Generally, the 12/48 V bidirectional DC-DC converter is installed in the vehicle engine room. For this reason, it is necessary to consider the case that the ambient temperature of the 12/48 V bidirectional DC-DC converter increases up to 125 °C [23]. Among the main power losses in DC-DC converter operation, the power loss caused by the switches is the largest. Therefore, this section analyzes the variation in the switching loss with the ambient temperature variation. For the designed 12/48 V bidirectional DC-DC converter switches (S_1, S_2), considering the high voltage spikes, IRFB4110PBF of *Infineon Technologies* was used. The loss occurring in the switches consists of the switching loss and conduction loss. The switching loss ($P_{sw,loss}$) is determined by the switching frequency (f_{sw}) and rising/falling time (t_{rising}, $t_{falling}$) of the switch drain to source voltage (V_{DS}).

$$P_{sw,loss} = 0.5 \times V_{DS} \times I_{DS} \times (t_{rising} + t_{falling}) \times f_{sw} \quad (1)$$

The rising/falling time is proportional to the switch internal capacitance. Even if the ambient temperature changes from 25 °C to 125 °C, the variation in the internal capacitance is less than 10 %. Thus, the variation in the rising/falling time of V_{DS} is less than 10 %. For this reason, the switching loss variation with ambient temperature variation can be omitted.

However, the conduction loss of the switch is greatly affected by the ambient temperature variation. The switch junction temperature (T_J) according to the ambient temperature (T_a) is as follows.

$$T_J = T_a + R_{\theta(j-a)} + R_{\theta(j-c)} + R_{\theta(c-s)} \quad (2)$$

where $R_{\theta(j-a)}$ is the switch junction to ambient thermal resistance, $R_{\theta(j-c)}$ is the switch junction to case thermal resistance

and $R_{\theta(c-s)}$ is the switch case to heat sink thermal resistance. $R_{\theta(j-a)}$, $R_{\theta(j-c)}$ and $R_{\theta(c-s)}$ are values that can be changed according to the heat dissipation system by the designers. Even if the values of $R_{\theta(j-a)}$, $R_{\theta(j-c)}$ and $R_{\theta(c-s)}$ are very small according to the heat dissipation system design, the variation in T_a directly affects T_J. Therefore, to analyze $R_{DS,on}$ and the variation rate in the conduction loss ($P_{Cond,loss}$) with the variation in T_a, this section assumed that the values of $R_{\theta(j-a)}$, $R_{\theta(j-c)}$ and $R_{\theta(c-s)}$ are very small due to the heat dissipation system using fans or a water cooling system. The $P_{Cond,loss}$ of switches (S_1, S_2) is calculated by the drain to source current (I_{DS}) and $R_{DS,on}$.

$$P_{Cond,loss} = I_{DS}^2 \times R_{DS,on} \tag{3}$$

In the case of T_a is equal to 25 °C, $R_{DS,on}$ is 3.7 mΩ, and $P_{Cond,loss}$ in each switch (S_1, S_2) is 83.25 W under the maximum load condition. When T_a rises to 125 °C according to the vehicle engine room temperature, $R_{DS,on}$ increases to approximately 6.7 mΩ. At this time, the $P_{Cond,loss}$ occurring in each switch (S_1, S_2) is approximately 148.5 W under the maximum load condition. The switch conduction loss variation with the ambient temperature is as follows, (4)–(6), as shown at the bottom of the page, Therefore, the variation in the conduction loss factor with the temperature variation of the switch is approximately 78.37 %.

In this section, the raw materials cost of the 12/48 V bidirectional DC-DC converter and the mechanical torque converter are compared by configuring the actual hardware. TABLE 3 shows the main components, quantities and cost of the 12/48 V bidirectional DC-DC converter designed based on TABLE 2. The total cost of the 12/48 V bidirectional DC-DC converter was set in TABLE 3 according to the costs from the online retailers (*Digikey*, *Mouser*).

The gear information of the planetary gears for proposed mechanical torque converter is shown in TABLE 4. The gear type of the mechanical torque converter is a spur gear type. The number of teeth of the sun gear, planetary gear and ring gear are 16 T, 32 T and 80 T, respectively. Each gear and shaft of the designed mechanical torque converter is made of SCM415 material for high gear strength and wear. SCM415 contains 0.13 ∼ 0.18 % carbon and is widely used in fields requiring high durability [24]. The frictional losses in gears are determined by the thermal expansion coefficient of the material with temperature variation. When SCM415 is applied to the mechanical torque converter, the thermal expansion coefficient is 12.2 μm/m°C. According to this thermal expansion coefficient, the variation in the thermal expansion coefficient with vehicle engine room temperature is very slight. Therefore, the proposed BSG with the mechanical torque converter can avoid the friction loss occurring in the gear according to the vehicle engine room temperature.

However, to configure the mechanical torque converter with SCM415, the inherent yield strength according to the temperature must be considered. Yield strength refers to the critical stress at which permanent deformation occurs.

TABLE 3. Main components and cost of the 12/48 V bidirectional DC-DC converter.

Component	Model	Quantity [EA]	Unit cost [$]	Cost [$]
Primary switch(S_1~S_2)	IRFB4110PBF	2	2.91	5.82
Secondary switch(S_3~S_6)	IPB80N07S4-05	4	1.22	4.88
Transformer	High flux ferrite (EE5555)	1	2.86	2.86
Primary capacitor	B32524	3	8.52	25.56
Secondary capacitor	B32529-D5335	4	0.43	1.72
Inductor	CH648125	1	13.5	13.5
Current sensor	APT100S20B(G)	2	7.18	14.36
Controller	TMS320F28335PGFA	1	25.99	25.99
Gate driver	IC-IXDD609SIA	6	1.65	9.9
Auxiliary power source	NTE0515	6	7.95	45.9
PCB	205mm*90mm 1.6T/2layer	1	14.63	14.63
Heat sink	ATS-EXL76-300-R0	1	66.21	66.21
	Total cost			231.33

TABLE 4. Gear Information of the proposed mechanical torque converter.

Description	Sun gear	Planetary gear	Ring gear	Unit
Gear type		Spur Gear		N/A
Material		SCM415		N/A
Pressure angle		20		[°]
Number of teeth	16	32	80	[T]
Reduction ratio		6		N/A
Torsion angle	20(Right)	20(Left)	20(Left)	[°]
Tooth width	13	11	14	[mm]
Raw material cost		3.0		[$/kg]
Total mass		11.17		[kg]
Total cost		33.51		[$]

$$\textit{Conduction loss factor at } 25^{\circ}\text{C} = \frac{83.25[\text{W}]}{1800[\text{W}]} \times 100\% = 4.625\% \tag{4}$$

$$\textit{Conduction loss factor at } 125^{\circ}\text{C} = \frac{148.5[\text{W}]}{1800[\text{W}]} \times 100\% = 8.25\% \tag{5}$$

$$\textit{Variation conduction loss factor} = \frac{\textit{Conduction loss factor at } 125^{\circ}\text{C} - \textit{Conduction loss factor at } 25^{\circ}\text{C}}{\textit{Conduction loss factor at } 25^{\circ}\text{C}} = 78.37\% \tag{6}$$

When the ambient temperature of the mechanical torque converter increases up to 125 °C according to the vehicle engine room temperature, the inherent yield strength of SCM415 is 600 MPa or higher [25]. Even though SCM415 has high strength, it is necessary to analyze the variation in yield strength and safety factor in order to apply it to the vehicle gear. The relationship between the yield strength and safety factor is as follows.

$$Safety\ factor = \frac{Yield\ stress}{Working\ stress} \times 100\% \tag{7}$$

where *Yield strength* means the inherent yield strength according to the temperature of the SCM415, and *Working stress* means the strength exhibited by the gear according to the conditions applied to the gear. In this case, assuming that *Working stress* is k, the variation in the safety factor according to the temperature variation of SCM415 can be derived. When the temperature of SCM415 is 25 °C and 125 °C, the inherent yield strengths of SCM415 are approximately 620 MPa and 610 MPa, respectively. The safety factor variation according to the temperature variation of SCM415 is as follows:

$$Safety\ factor\ at\ 25^{o}C = \frac{620\ [MPa]}{k} \times 100\% \tag{8}$$

$$Safety\ factor\ at\ 125^{o}C = \frac{610\ [MPa]}{k} \times 100\% \tag{9}$$

$$Variation\ safety\ factor = \frac{Safety\ factor\ at\ 25\ ^{o}C – Safety\ factor\ at\ 125\ ^{o}C}{Safety\ factor\ at\ 25\ ^{o}C} = 1.64\% \tag{10}$$

Therefore, since the variation in the safety factor according to the temperature variation of SCM415 is approximately 1.64 %, it can be derived that SCM415 has sufficient durability according to the temperature variation.

With the ambient temperature variation, the 12/48 V bidirectional DC-DC converter affects the electrical characteristics, and the mechanical torque converter affects the mechanical characteristics. In the case of the 12/48 V bidirectional DC-DC converter, the electrical characteristic (conduction loss factor) variation with the ambient temperature variation is 78.37 %. However, in the case of the mechanical torque converter, the mechanical characteristic (safety factor) variation with the ambient temperature variation is 1.64 %. Therefore, the mechanical torque converter can operate more stably than the 12/48 V bidirectional DC-DC converter.

The weight of the planetary gears is 11.17 kg, as presented in TABLE 4; thus, the percentage change in the micro-HEV weight is slight. In addition, the fuel economy variation with installation of the mechanical torque converter can be derived [26].

$$Fuel\ economy = –0.01 \times Vehicle\ weight\ + 117 \tag{11}$$

TABLE 5. Target characteristics of 12 V BSG operation.

Mode	Description	Value	Unit
Starter (CW)	Starting torque	9.5	[N·m]
	Starting speed	1,200	[rpm]
Generator (CCW)	Maximum power generation	1.8	[kW]
	Output voltage	15.6	[V]
	Rated speed	2,000 ~3,000	[rpm]
	Maximum speed	10,000	[rpm]

Assuming that the weight of the typical micro HEV is 1,500 kg, the fuel economy variation with the installation of the mechanical torque converter is derived as approximately 0.001 %. Therefore, it is considered that the influence of the fuel economy change due to the mechanical torque converter weight in a micro-HEV is insignificant.

Based on the comparison and analysis, a 12 V BSG system using a mechanical torque converter can be constructed simply with a lower cost. When comparing the maintenance cost incurred by component replacement due to fault and wear of the DC-DC converter and the planetary gear, the cost of failure-prone components of the DC-DC converter such as switches, capacitors and drivers is higher than the manufacturing cost of the mechanical torque converter, as presented in TABLE 3 and TABLE 4. Therefore, when a mechanical torque converter is mounted on a 12 V BSG system, it is possible to operate the BSG system with high durability while solving the unit cost issue of the boost-type BSG system.

B. COMPARISON OF MOTOR TYPES FOR 12 V BSG SYSTEM

In case the of a belt-driven integrated starter and generator (BSG), a permanent magnet synchronous machine (PMSM) and a wound field synchronous machine (WFSM) are generally used. A PMSM has the advantages of high torque and high efficiency [27], [28].

However, in the micro-HEV using a 12 V BSG, the input voltage for driving the BSG is low. Thus, it is necessary to test whether the PMSM is applicable to the 12 V BSG system. In this section, whether the PMSM is applicable to the 12V BSG is tested based on the required characteristics (torque and voltage limit in a high speed range). TABLE 5 lists the target characteristics of the 12 V BSG system.

The voltage limit value (V_{limit}) of the motor is generally determined by the input voltage and the control method. There are typically three control methods: space vector pulse width modulation (SVPWM), sinusoidal pulse width modulation (SPWM) and the 6-step control method [29]–[31]. According to control methods (SVPWM, SPWM and 6-step), the voltage limit values with a 12 V input voltage are shown in TABLE 6. The stator phase voltage (V_{abc}) is derived through the stator phase voltage equation. When V_{abc} exceeds V_{limit}, operating the motor is impossible. The output

TABLE 6. Voltage limit value according to the control methods.

Control method	SVPWM	SPWM	6-step	Unit
Voltage limit	$\frac{V_{DC}}{\sqrt{3}}$	$\frac{V_{DC}}{2}$	$\frac{2}{\pi}V_{DC}$	[V]
Voltage limit value	6.93	6	7.64	[V]

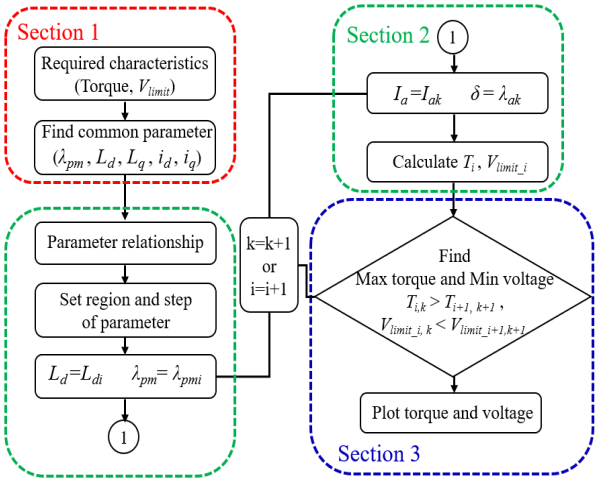

FIGURE 3. Algorithm for deriving the maximum output torque and minimum stator phase voltage.

torque(T) can be calculated by the parameters from the stator phase voltage equation.

$$V_{abc} = \omega_r \sqrt{\left(L_d i_d + \lambda_{pm}\right)^2 + \left(L_q i_q\right)^2} \leq V_{limit} \quad (12)$$

$$T = \frac{3}{2} p \left(\lambda_{pm} i_q + \left(L_d - L_q\right) i_d i_q\right) \quad (13)$$

where L_d is the d-axis inductance of the rotor, L_q is the q-axis inductance of the rotor, i_d and i_q are the d-axis and q-axis currents of the stator, respectively, ω_r is the rotor electrical angular velocity, p is the numbers of poles and λ_{pm} is the magnet flux from the permanent magnet.

Fig. 3 shows an algorithm that shows how to find the maximum output torque (T) and minimum stator phase voltage (V_{abc}). In Fig. 3, Section 1 represents a process for finding common parameters from output torque and stator phase voltage equations. Section 2 represents a process for reducing the number of parameters using relationships of parameters (L_d, L_q, i_d and i_q). These parameters have a dependent relationship with each other. The following equations show the dependent relationships of these parameters (L_d, L_q, i_d and i_q).

$$\delta = \frac{L_q}{L_d} \quad (14)$$

$$i_d = -I_a \sin\beta \quad (15)$$

$$i_q = I_a \cos\beta \quad (16)$$

$$\frac{\partial T}{\partial \beta} = \frac{3}{2} p \left(-\lambda_{pm} I_a \sin\beta + \left(L_d - L_q\right) I_a^2 \cos 2\beta\right) = 0 \quad (17)$$

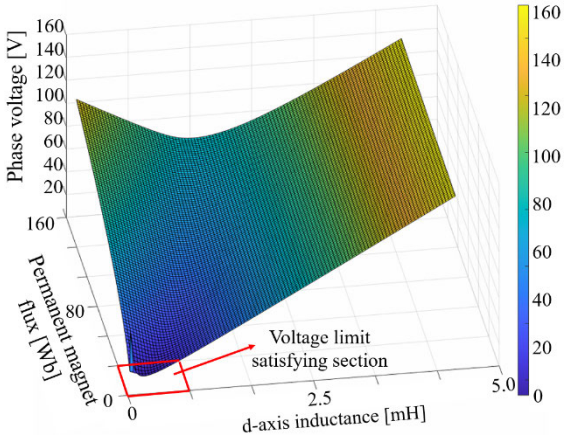

FIGURE 4. Stator phase voltage distribution at the rated speed.

where δ is the inductance ratio, I_a is the stator phase current and β is the angle at which the maximum torque occurs. This section uses inductance ratio values that lie within the range of the PMSM (1.2 to 2.5) [32]. In addition, it is possible to calculate the d-axis and q-axis inductance of the rotor by using I_a and β. β is determined as the angle at which the maximum torque occurs within the angle range of $0 \sim 90$. In (17), β is calculated from λ_{pm}, L_d, L_q and I_a. By selecting the region of the inductance ratio, β and variable combinations (L_d, I_a and λ_{pm}), it is possible to derive the output torque and stator phase voltage distribution. However, it is difficult to show the distribution using 3 variables (L_d, I_a and λ_{pm}). Therefore, this paper, an additional condition (I_a range: $0 \sim 20$ A) is added to present the distribution map. In Fig. 3, Section 3 represents comparing each output torque and stator phase voltage obtained for different combinations of parameters (L_d, I_a and λ_{pm}). When the maximum output torque and minimum stator phase voltage are determined, it is possible to derive the distribution map.

Through these distribution maps, it can be determined whether the PMSM motor satisfies the target specification conditions (torque and voltage limit in a high speed range). With the combination of these 3 variables (L_d, I_a and λ_{pm}), voltage and torque distribution graphs can be obtained as shown in Fig. 4 and Fig. 5. The PMSM has a section that satisfies the voltage limit value at the maximum speed (10,000 rpm) as shown in Fig. 4. However, the torque required for the maximum speed (10,000 rpm) does not lie in the voltage limit satisfying section, as shown in Fig. 5.

To satisfy the required torque at the maximum speed, the stator current must be increased. Fig. 6 shows the voltage limit ellipse and armature current limit circle according to the speed of the PMSM. The voltage limit ellipse equation is (12), and the armature current limit circle equation is $I_{a^2} = I_{d^2} + I_{q^2}$. The range of the voltage limit ellipse is inversely proportional to the speed of the PMSM. As the speed increases, the overlap with the armature current limit circle decreases. To operate the motor, the voltage limit ellipse should produce a crossing point with the armature current limit circle.

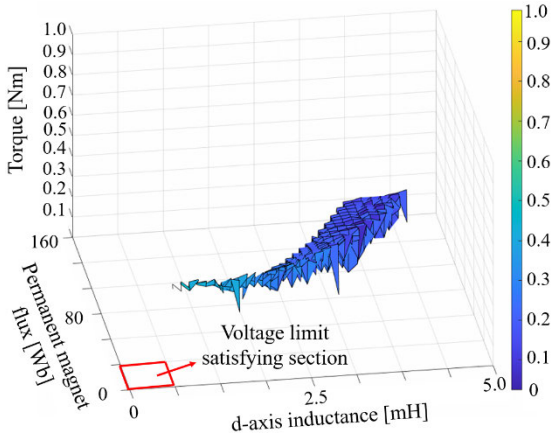

FIGURE 5. Maximum torque distribution at the maximum speed.

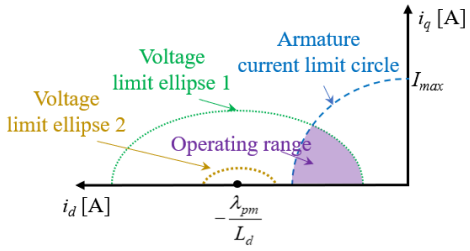

Operating speed
Voltage limit ellipse 1 < Voltage limit ellipse 2

FIGURE 6. Variations in PMSM voltage limit ellipse and armature current limit circle.

However, if the speed of the PMSM continues to increase, then a crossing point does not occur (see voltage limit ellipse 2 in Fig. 6). In this case, the voltage limit ellipse must be moved to the right or the armature current limit circle must be increased to produce a crossing point. Considering the voltage limit, it is impossible to increase the size of the armature current limit circle. Therefore, it is appropriate to move the center point of the voltage limit ellipse to the right. The center point of the voltage limit ellipse is determined by the magnetic flux of the rotor (λ_{pm}). However, the PMSM magnetic flux of the rotor (λ_{pm}) is determined by the permanent magnet. Therefore, to solve this problem, the WFSM which can control the field flux (λ_f), is used. Replacing λ_{pm} with λ_f, the voltage limit ellipse equation of the WFSM is as follows.

$$\frac{\left(i_d + \frac{\lambda_f}{L_d}\right)^2}{\left(\frac{V_{\max}}{\omega_r L_d}\right)^2} + \frac{i_q^2}{\left(\frac{V_{\max}}{\omega_r L_q}\right)^2} = 1 \tag{18}$$

Fig. 7 shows the WFSM voltage limit ellipse and current limit circle. As the magnitude of the field flux decreases (field current decreases), the value of λ_f / L_d decreases. Thus, the center of the voltage limit ellipse moves to the right and close to the origin and the armature current limit circle (see voltage limit ellipse 2 in Fig. 7). Through this field-current control, the WFSM can be operated at high speed with a limited input voltage (12 V).

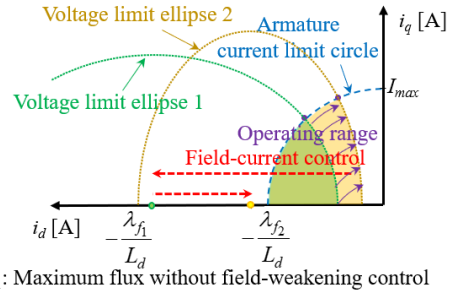

λ_1: Maximum flux without field-weakening control
λ_2 : Flux with field-weakening control

FIGURE 7. Variations in WFSM voltage limit ellipse and armature current limit circle.

TABLE 7. Parameters of the 12 V WFSM BSG design.

Parameter name	Value	Unit
Stator outer diameter	144	[mm]
Rotor outer diameter	100	[mm]
Stack length	50	[mm]
Material	50PN470	N/A
Numbers of poles and slots	12 and 36	N/A
Number of turns per slot (stator)	11	[turns]
Winding method	Delta	N/A
Number of turns per slot (rotor)	60	[turns]
Shaft inner diameter	14	[mm]
Operating temperature	-45 to 120	[°C]

For these reasons, in this paper, the WFSM was applied to the 12 V BSG requiring a wide operating range of power generation under various load conditions. The parameters of the 12 V WFSM BSG are listed in TABLE 7. In addition, by considering the magnitude of the non-load back electromotive force (back EMF) and the air magnetic flux density, a 12-pole, 36-slot, 6-step model with a concentric winding method was selected. Because the available battery voltage of micro-HEVs is very low, a delta connection (i.e., Δ connection) was chosen to increase the voltage utilization rather than a Y connection.

C. 12 V WFSM BSG SYSTEM WITH A MECHANICAL TORQUE CONVERTER

Fig. 8 illustrates the detailed size and configuration of the proposed 12 V WFSM BSG with a mechanical torque converter, and TABLE 8 lists gear ratios of the 12 V WFSM BSG. Gear information of the planetary gears is shown in TABLE 4. The belt-type pulley connected to the planetary gears has a 2:1 gear ratio in starter-mode and a 1:2 gear ratio in generator-mode. For the mechanical torque converter, a 6:1 planetary gear ratio is used in starter-mode, and a 1:1 planetary gear ratio is used in the generator-mode. Therefore, for the proposed BSG with a mechanical torque converter system, its gear ratios are 12:1 in starter-mode (i.e., the clockwise direction) and 1:2 in generator-mode (i.e., the counterclockwise direction) when a pulley is considered, as depicted in Fig. 8.

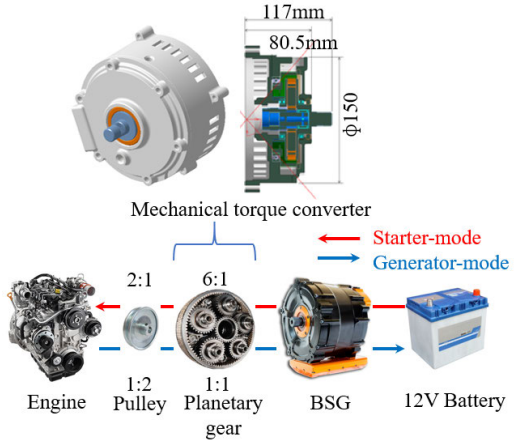

FIGURE 8. Configuration of the proposed 12 V WFSM BSG system.

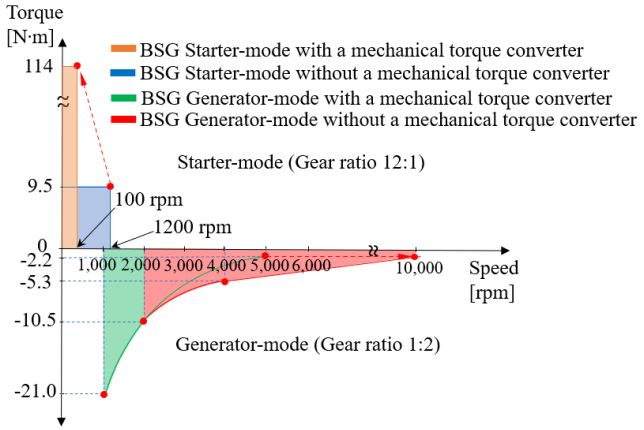

FIGURE 9. Load characteristic torque–speed curves of the proposed WFSM BSG system with the mechanical torque converter.

Because of the high gear ratio, the low starting torque issue with the 12 V BSG can be resolved with the mechanical torque converter. However, a WFSM BSG requires either a brush and slip-ring assembly or a brushless exciter to supply its field current. A brush and slip-ring assembly may cause abrasion, and a brushless-exciter-type WFSM has size and control issues [6]. To decrease the overall size of the system and simplify its control, we used a brush and slip-ring assembly to supply the field current with a 12 V battery in the proposed 12 V WFSM BSG system. To reduce the wear rate of the system brush and slip-ring assembly, we used carbon brushes with higher rated current and sufficient hardness to guarantee reliable operation of the proposed 12 V WFSM BSG system during the lifetime of the micro-HEV. The simple structure, simple control method, and highly durable material of the 12 V WFSM BSG can overcome the maintenance issues of a mechanical torque converter.

Fig. 9 presents the load characteristic curves of the proposed BSG with the mechanical torque converter in starter and generator modes. The starting torque required for the target micro-HEV engine is above 100 N·m. To achieve the required high starting torque, the conventional BSG with

TABLE 8. Gear ratios of the proposed 12 V WFSM BSG.

Mode	Description	Value
Starter (CW)	Pulley	2:1
	Planetary gear	6:1
	Pulley + Planetary gear	12:1
Generator (CCW)	Pulley	1:2
	Planetary gear	1:1
	Pulley + Planetary gear	1:2

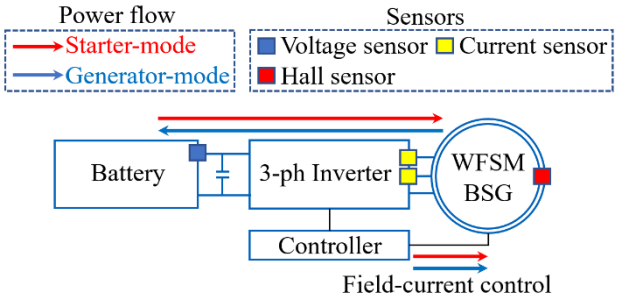

FIGURE 10. Proposed 12 V WFSM BSG control method without a voltage-boosting converter.

a 12 V battery requires a high discharge current from the battery in a short time; this may exceed the battery capacity. However, the required starting torque of the 12 V WFSM BSG is approximately 9.5 N·m when the starting speed of the motor is 1,200 rpm as shown in Fig. 9. Because the gear ratio including the pully and planetary gears is 12:1 in starter-mode as given in TABLE 8, the required driving current for the 12 V WFSM BSG is significantly less than that for the conventional BSG; thereby, the battery capacity shortage issue is possibly resolved by using the mechanical torque converter. In addition, the target micro-HEV engine speed in the idle state is maintained at 1,000 rpm, and its maximum engine speed is 5,000 rpm. Depending on the engine type, the maximum speed can increase to a value exceeding 5,000 rpm. Based on the 1:2 gear ratio including the pully and planetary gears, the proposed WFSM BSG was designed to satisfy the power generation speed range (10,000 rpm) as depicted in the generator-mode of Fig. 9. The proposed WFSM BSG generates above 15 V for charging a 12 V battery in generator-mode.

III. 12 V WFSM BSG SIMULATION

Fig. 10 presents the bidirectional control algorithm for the WFSM BSG simulation analysis using the field-current control method. The existing reinforced starter for the BSG has no separate controller, and its regulator controls the field current to maintain a constant voltage with various engine speeds in generator-mode. The starting torque requirement for the proposed 12 V WFSM BSG in starter-mode can be satisfied with a torque control method by detecting its rotor position with Hall sensors. The WFSM simulation analysis of the proposed field-current control method is divided into starter and generator modes.

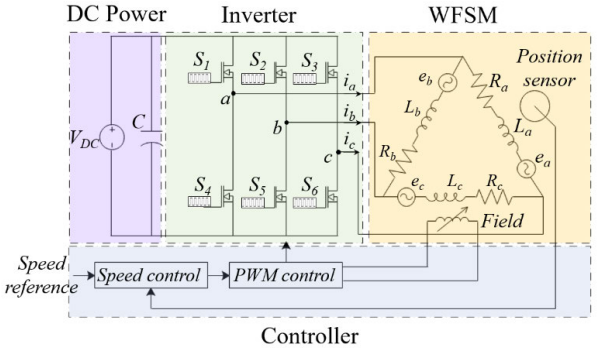

FIGURE 11. Equivalent circuit model for WFSM starter-mode.

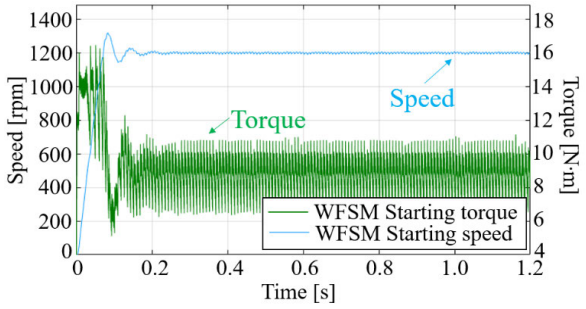

FIGURE 12. Starter-mode simulation results.

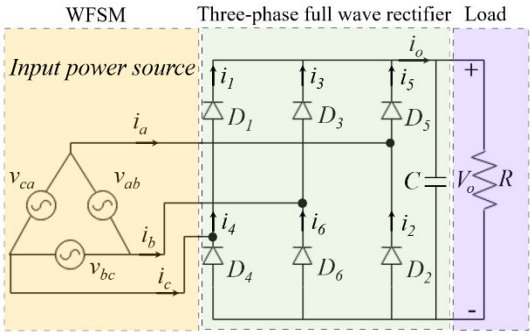

FIGURE 13. Equivalent circuit model for the WFSM generator-mode.

A. STARTER-MODE SIMULATION RESULTS

The WFSM BSG must satisfy the required starting torque of 9.5 N·m at 1,200 rpm in starter-mode, given the pulley and planetary gear ratio of the WFSM BSG. Because a starter-mode simulation can be performed by using voltage source analysis with the BLDC motor control method, a BLDC motor drive circuit was used for the voltage source analysis as shown in Fig. 11. Each phase voltage equation of the WFSM stator and field winding in starter-mode can be expressed as follows.

$$\begin{aligned}\begin{bmatrix} v_a & v_b & v_c & v_f \end{bmatrix}^T &= R_s \begin{bmatrix} i_a & i_b & i_c & i_f \end{bmatrix}^T \\ &+ (L_s - M)\frac{d}{dt}\begin{bmatrix} i_a & i_b & i_c & i_f \end{bmatrix}^T \\ &+ \begin{bmatrix} e_a & e_b & e_c & e_f \end{bmatrix}^T \end{aligned} \tag{19}$$

where the stator phase voltage and current are $v_{abc} = [v_a\ v_b\ v_c]^T$ and $i_{abc} = [i_a\ i_b\ i_c]^T$, respectively, v_f and i_f are the field winding voltage and current, respectively, R_s is the stator resistance, L_s is the inductance of the stator including the magnetic inductance and the leakage inductance, e_a, e_b, and e_c are the back EMFs of each phase of the stator and e_f is the back EMF of the field winding. A mathematical model of the WFSM BSG was constructed using MATLAB/Simulink to test the WFSM BSG for the target specifications in starter-mode. For verification of the starter-mode algorithm using the mathematical model and the parameters of the 12 V WFSM BSG listed in TABLE 7, the starting torque was simulated. As shown in Fig. 12, the starting torque reached 9.5 N·m at 1,200 rpm, which satisfied the target specifications in this study.

B. GENERATOR-MODE SIMULATION RESULTS

The WFSM BSG charges the vehicle battery according to the field current and generating torque conditions in generator-mode. For the generator-mode analysis, the three-phase full wave rectifier circuit was constructed as shown in Fig. 13, and the condition in which the amount of power generated varies according to the field current and generating torque was simulated. In the case of a delta connection, the phase voltage and the line voltage are the same. Each diode in the upper group of diodes (D_1, D_3, and D_5) has a 120° phase difference between their conduction currents. In addition, each diode in the lower group of diodes (D_2, D_4 and D_6) has a 120° phase difference between their conduction currents. Therefore, the average value of the output voltage is expressed as follows.

$$\begin{aligned}\langle v_o \rangle &= \frac{3}{\pi}\int_0^{\frac{\pi}{3}} v_{cb} d(\omega t) \\ &= -\frac{3}{\pi}\int_0^{\frac{\pi}{3}} \sqrt{2}V \sin(\omega t - \frac{2}{3}\pi) d(\omega t) = \frac{3\sqrt{2}V}{\pi}\end{aligned} \tag{20}$$

To verify the generator-mode algorithm for the WFSM BSG, a three-phase full wave rectifier circuit was used by constructing a WFSM BSG MATLAB/Simulink model in generator-mode. In generator-mode, as shown in Fig. 14, the maximum power generation is 1.8 kW at a field current of 53 A and a generating torque of 10.5 N·m. This power generation from the WFSM BSG is used for charging the battery in generator-mode.

By applying the finite element method with ANSYS Electromagnetic 19.0 to the generator-mode of the WFSM BSG, the output voltage, output current, and efficiency maps over the operating speed range of the WFSM BSG were obtained, as shown in Figs. 15. Because the output voltage of the WFSM BSG increases with increasing speed, its field current decreases to generate the same voltage. As shown in Fig. 15(a), the field current to generate the same voltage decreases as the WFSM BSG speed increases. Thus, the output voltage satisfies the required voltage generation. As shown in Fig. 15(b), the output current of the WFSM BSG is greater than 100 A from 2,000 rpm. In addition,

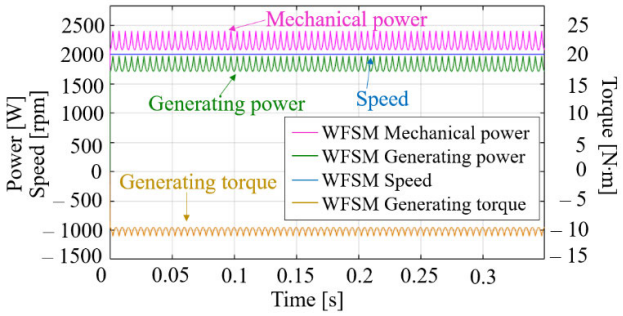

FIGURE 14. Simulation results of the WFSM in generator-mode (1.8 kW at 2,000 rpm; torque of −10.5 N·m).

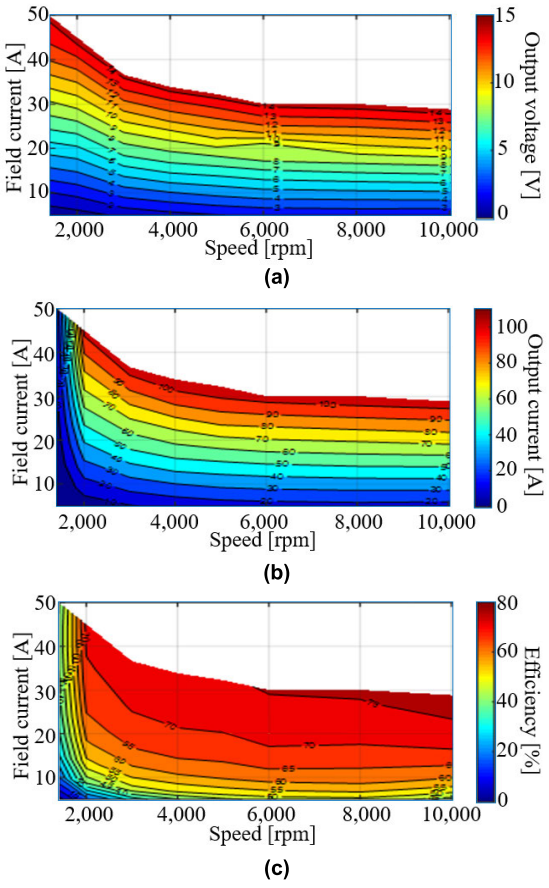

FIGURE 15. WFSM generator-mode simulation results with the finite element method: (a) Output voltage map (b) Output current map (c) Efficiency map.

the output current can satisfy the maximum power generation considering the output voltage. Fig. 15(c) presents the maximum power generation efficiency map of the proposed WFSM BSG.

IV. 12 V WFSM BSG EXPERIMENTAL RESULTS

To verify the performance of the proposed 12 V WFSM BSG with a mechanical torque converter system, a 12 V WFSM BSG load and generation test system with an electric motor–generator dynamometer was constructed in the laboratory. In a belt-type micro-HEV, a pulley is used to connect

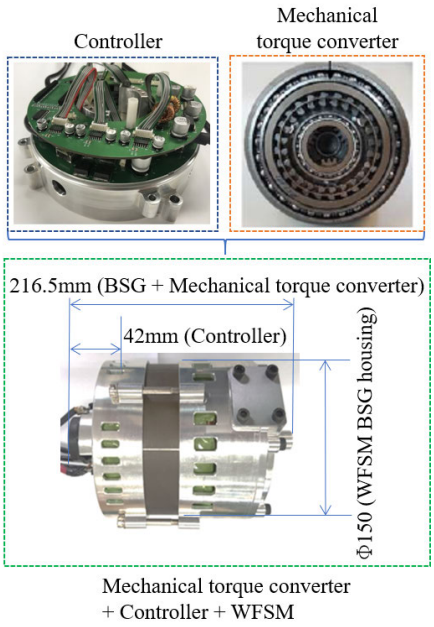

FIGURE 16. Proposed WFSM BSG system assembled with a mechanical torque converter and a field current–driving control board.

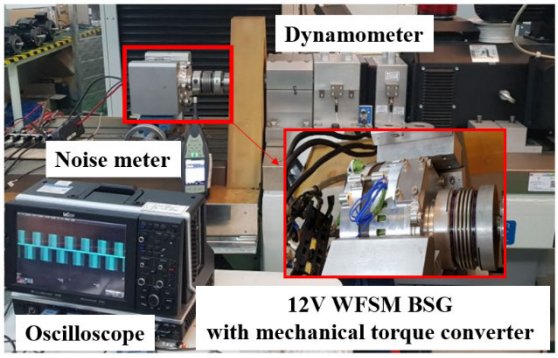

FIGURE 17. WFSM BSG generation dynamometer test set.

the BSG and the engine with a belt. Because the electric motor–generator dynamometer test was conducted instead of an engine test with a micro-HEV, a pulley and a belt were not used; only planetary gears were used under the starter-mode and generator-mode test conditions of the dynamometer test bench. To realize the engine rotation speed, the test was performed using the rotation speed of the dynamometer load system by considering the pulley ratio. The planetary gear ratios in starter-mode (i.e., 6:1) and generator-mode (i.e., 1:1) in TABLE 8 were used for the mechanical torque converter of the BSG in the dynamometer test bench environment.

As shown in Fig. 16, a field current–driving control board was integrated into the 12 V WFSM BSG system, and the mechanical torque converter could be attached to the front of the WFSM BSG. Therefore, the 12 V WFSM BSG system could be installed in the limited space of a micro-HEV engine room. Fig. 17 presents the load and generation test environments of the proposed 12 V WFSM BSG with a mechanical torque converter to verify its field-current control capability.

TABLE 9. WFSM Starter-mode test results.

Description		Value	Unit
BSG	Starting torque	9.59	[N·m]
	Starting speed	1,227	[rpm]
BSG + Planetary gear	Starting torque	50.97	[N·m]
	Starting speed	201.8	[rpm]
Efficiency of planetary gears		87.4	[%]

To verify the field-current control performance, starter-mode and generator-mode tests in which a bidirectional DC power supply was used were performed.

A. STARTER-MODE TEST RESULTS

The starter-mode test results presented in TABLE 9 were obtained from the dynamometer load test for the 12 V WFSM BSG itself (i.e., the motor performance test) and the load test for the BSG with the planetary gears (i.e., the BSG system performance test). Because the starter-mode of the vehicle is driven in a very short time, it is important to instantly satisfy the required torque in the starter-mode of the proposed 12 V WFSM BSG considering the gear ratio. Thus, the starter-mode test of the proposed WFSM BSG was focused on whether the required torque is satisfied in starter-mode. The results of this WFSM BSG system in the starter-mode experiment exhibit good agreement with the MATLAB/Simulink results presented in Fig. 12 and the target specifications presented in Fig. 9, which are a set of BSG system requirements used to generate the torque (9.5 N·m at 1,200 rpm) required for the starter performance.

Therefore, the starter-mode experiment verifies that the proposed WFSM BSG system can be used as a BSG system of a micro HEV. In addition, the efficiency of the planetary gears (i.e., mechanical torque converter) was estimated to be 87.4 % by comparing the motor power (i.e., the product of the torque and speed) from the BSG single component and that from the BSG combined with the planetary gears. Although the efficiency of the mechanical torque converter is slightly less than that of a voltage-boosting power converter (approximately 90 %), the proposed 12 V WFSM BSG with a mechanical torque converter is a more cost-effective solution than the conventional BSG using a DC-DC converter (as shown in TABLE 1).

B. GENERATOR-MODE TEST RESULTS

To test the generator-mode performance, a DC current was applied to the field winding of the WFSM. The WFSM was rotated by the dynamometer to measure the output voltage and current through the controller. In the generator-mode test, field currents were applied to generate an output voltage greater than 15 V while the speed of the WFSM varied from 2,000 to 10,000 rpm.

Fig. 18 presents the output voltage and output current according to the proposed 12 V WFSM BSG speed

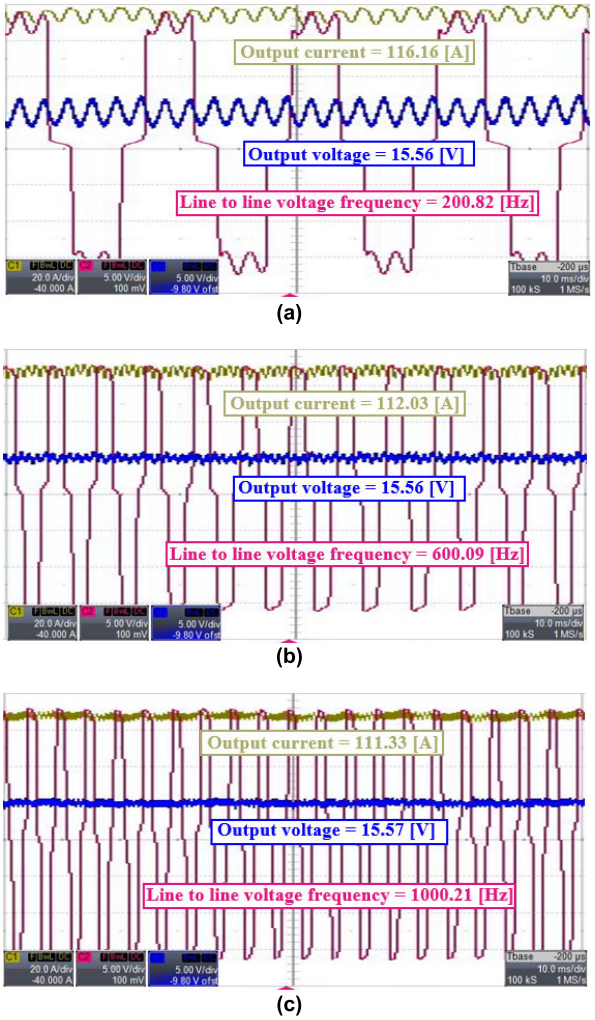

FIGURE 18. WFSM BSG test results in generator-mode: (a) WFSM BSG speed: 2,000 rpm (b) WFSM BSG speed: 6,000 rpm (c) WFSM BSG speed: 10,000 rpm.

(2,000 to 10,000 rpm). To measure the rotation speed of the proposed WFSM BSG, the frequency of the stator line to line voltage was measured. Then, the measured frequency of the stator line to line voltage was converted to the rotation speed of the proposed WFSM BSG. According to Fig. 18, the output current decreases as the rotation speed of the WFSM BSG increases. However, the output voltage for battery charging is maintained above 15 V in generator-mode.

Fig. 19 presents the measured generator-mode test data of the 12 V WFSM BSG including the output voltage, output current, power efficiency, field current, power generation, and generating torque. Given that the pulley gear ratio is 1:2 in generator-mode, the generator-mode test of the 12 V WFSM BSG was conducted over its full speed range, which is up to 10,000 rpm, as shown in Fig. 19. This is a reasonable test because the operating speed range of the BSG must be twice that of a micro-HEV engine (i.e., up to 5,000 rpm) when the pulley ratio of the generator-mode is considered. In the idle state of the BSG (i.e., 2,000 rpm), a high field current is required to generate an output voltage greater

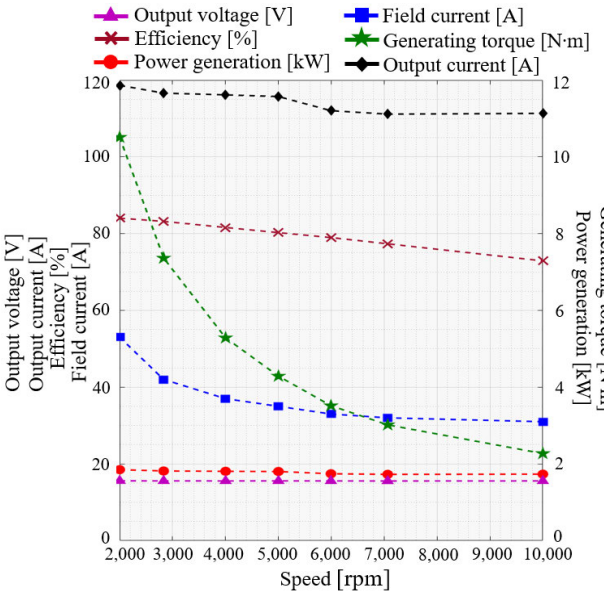

FIGURE 19. WFSM BSG test results at various speeds in generator-mode.

than 15 V. These generator-mode experimental results for the 12 V WFSM BSG system also exhibit good agreement with the finite element method results of ANSYS Electromagnetic 19.0 presented in Fig. 15. Therefore, the generator-mode experiment verified that the proposed WFSM BSG system can be used as a BSG system of a micro-HEV.

V. CONCLUSION

In this paper, a 12 V WFSM with a mechanical torque converter was proposed for a BSG system of micro-HEVs without an additional DC-DC converter. The conclusions of this study are summarized as follows:

- By replacing a 12/48 V bidirectional DC-DC converter with a structurally simple mechanical torque converter, the proposed 12 V WFSM BSG system becomes a cost-effective system. In addition, through the comparison analysis according to the ambient temperature variation, the proposed mechanical torque converter achieves a lower influence with ambient temperature variations than the bidirectional DC-DC converter.
- To determine the type of 12 V BSG motor, an algorithm was proposed in this paper to derive the maximum output torque and the minimum stator phase voltage of the PMSM and WFSM. By using the proposed algorithm, it was concluded that the WFSM has the advantage in high-speed operation, thus it was applied to the proposed 12V BSG system.
- Simulation and experimental results demonstrated that this 12 V WFSM BSG with a mechanical torque converter satisfies the required starting torque in starter-mode and has a wide generation range under various load conditions in generator-mode.

Therefore, the proposed 12 V WFSM with a mechanical torque converter can provide an efficient solution to the high cost issue and temperature effects incurred by a micro-HEV that requires an additional DC-DC converter system.

REFERENCES

[1] E. Trancho, E. Ibarra, A. Arias, I. Kortabarria, J. Jurgens, L. Marengo, A. Fricasse, and J. V. Gragger, "PM-assisted synchronous reluctance machine flux weakening control for EV and HEV applications," *IEEE Trans. Ind. Electron.*, vol. 65, no. 4, pp. 2986–2995, Apr. 2018.

[2] C. Tong, M. Wang, P. Zheng, J. Bai, and J. Liu, "Characteristic analysis and functional validation of a brushless flux-modulated double-rotor machine for HEVs," *IEEE Trans. Ind. Electron.*, vol. 66, no. 1, pp. 663–673, Jan. 2019.

[3] Z. Zhang, A. Rick, and B. Sisk, "Model development and simulations of 12 V dual batteries towards design optimization of microhybrid vehicles," SAE Tech. Paper 2015-01-1199, 2015.

[4] C. S. Kim, K. Park, H. Kim, G. Lee, K. Lee, H. J. Yang, H. Cho, M. Song, and Y. Son, "48 V power assist recuperation system (PARS) with a permanent magnet motor, inverter and DC-DC converter," in *Proc. 1st Int. Future Energy Electron. Conf. (IFEEC)*, Tainan, Taiwan, Nov. 2013, pp. 137–142.

[5] R. R. Henry, B. Lequesne, S. Chen, J. J. Ronning, and Y. Xue, "Belt-driven starter-generator for future 42-volt systems," SAE Tech. Paper 2001-01-0728, 2001.

[6] N. Jiao, W. Liu, Z. Zhang, T. Meng, J. Peng, and Y. Jiang, "Field current estimation for wound-rotor synchronous starter–generator with asynchronous brushless exciters," *IEEE Trans. Energy Convers.*, vol. 32, no. 4, pp. 1554–1561, Dec. 2017.

[7] X. Hu, J. Zhou, and X. Cheng, "Transient simulation for an ISG HEV dual-voltage 42 V/14 V power-net system," in *Proc. Int. Conf. Energy Environ. Technol.*, Guilin, China, 2009, pp. 491–496.

[8] Y. Zhang, X. Cheng, C. Yin, and S. Cheng, "A soft-switching bidirectional DC-DC converter for the battery super-capacitor hybrid energy storage system," *IEEE Trans. Ind. Electron.*, vol. 65, no. 10, pp. 7856–7865, Oct. 2018.

[9] M.-S. Huang, K.-C. Chen, T.-K. Chen, Y.-C. Liang, and G.-Y. Pan, "An innovative constant voltage control method of PMSM-type ISG under wide engine speed range for scooter with idling stop," *IEEE Access*, vol. 7, pp. 20723–20733, Jan. 2019.

[10] J. Lara, J. Xu, and A. Chandra, "Effects of rotor position error in the performance of field-oriented-controlled PMSM drives for electric vehicle traction applications," *IEEE Trans. Ind. Electron.*, vol. 63, no. 8, pp. 4738–4751, Aug. 2016.

[11] J. Liu, C. Gong, Z. Han, and H. Yu, "IPMSM model predictive control in flux-weakening operation using an improved algorithm," *IEEE Trans. Ind. Electron.*, vol. 65, no. 12, pp. 9378–9387, Dec. 2018.

[12] Y. Nie, I. P. Brown, and D. C. Ludois, "Deadbeat-direct torque and flux control for wound field synchronous machines," *IEEE Trans. Ind. Electron.*, vol. 65, no. 3, pp. 2069–2079, Mar. 2018.

[13] S. Utegenova, F. Dubas, M. Jamot, R. Glises, B. Truffart, D. Mariotto, P. Lagonotte, and P. Desevaux, "An investigation into the coupling of magnetic and thermal analysis for a wound-rotor synchronous machine," *IEEE Trans. Ind. Electron.*, vol. 65, no. 4, pp. 3406–3416, Apr. 2018.

[14] Y. Lei, J. Lin, M. J. Zuo, and Z. He, "Condition monitoring and fault diagnosis of planetary gearboxes: A review," *Measurement*, vol. 48, pp. 292–305, Feb. 2014.

[15] G. Tang, W. Kong, and T. Zhang, "The investigation of multiphase motor fault control strategies for electric vehicle application," *J. Electr. Eng. Technol.*, vol. 15, no. 1, pp. 163–177, Oct. 2019.

[16] D. Uzel, Z. Peroutka, V. Smidl, T. Kosan, and K. Zeman, "Self-sensing control of wound rotor synchronous motor drive for mine hoist," *IEEE Trans. Ind. Electron.*, vol. 65, no. 3, pp. 2009–2017, Mar. 2018.

[17] R. Cao, X. Yuan, Y. Jin, and Z. Zhang, "MW-class stator wound field flux-switching motor for semidirect drive wind power generation system," *IEEE Trans. Ind. Electron.*, vol. 66, no. 1, pp. 795–805, Jan. 2019.

[18] Y. Zhou, H. Li, H. Zhang, J. Mao, and J. Huang, "Model free deadbeat predictive speed control of surface-mounted permanent magnet synchronous motor drive system," *J. Electr. Eng. Technol.*, vol. 14, no. 1, pp. 265–274, Jan. 2019.

[19] A. K. Jain and V. T. Ranganathan, "Modeling and field oriented control of salient pole wound field synchronous machine in stator flux coordinates," *IEEE Trans. Ind. Electron.*, vol. 58, no. 3, pp. 960–970, Mar. 2011.

[20] K. Yamamoto, E. Hiraki, T. Tanaka, M. Nakaoka, and T. Mishima, "Bidirectional DC-DC converter with full-bridge/push-pull circuit for automobile electric power systems," in *Proc. 37th IEEE Power Electron. Spec. Conf.*, Jeju, South Korea, Jun. 2006, pp. 1–5.
[21] F. J. Nome and I. Barbi, "A ZVS clamping mode-current-fed push-pull DC-DC converter," in *Proc. IEEE Int. Symp. Ind. Electron.*, vol. 2, Jul. 1998, pp. 617–621.
[22] K. Kim, H.-W. Kim, K. Lee, and J. Park, "Gate driver for SiC power MOSFETs using soft-switching technique," *J. Electr. Eng. Technol.*, vol. 14, no. 3, pp. 1311–1319, Feb. 2019.
[23] N. Zhao, N. Schofield, R. Yang, and R. Gu, "Investigation of DC-link voltage and temperature variations on EV traction system design," *IEEE Trans. Ind. Appl.*, vol. 53, no. 4, pp. 3707–3718, Jul. 2017.
[24] H. Onozuka, F. Tayama, Y. Huang, and M. Inui, "Cutting force model for power skiving of internal gear," *J. Manuf. Processes*, vol. 56, pp. 1277–1285, Aug. 2020.
[25] N.-A. Noda, D. Suryadi, S. Matsuda, Y. Sano, and Y. Takase, "Proposal for new hearth roller consisting of ceramic sleeve and steel shafts used in the heat treat furnace," *ISIJ Int.*, vol. 55, no. 11, pp. 2416–2425, 2015.
[26] H. Jung, "Fuel economy of plug-in hybrid electric and hybrid electric vehicles: Effects of vehicle weight, hybridization ratio and ambient temperature," *World Electr. Vehicle J.*, vol. 11, no. 2, p. 31, Mar. 2020.
[27] X. Liu, H. Yu, J. Yu, and Y. Zhao, "A novel speed control method based on port-controlled Hamiltonian and disturbance observer for PMSM drives," *IEEE Access*, vol. 7, pp. 111115–111123, Aug. 2019.
[28] J. Wu, J. Wang, C. Gan, Q. Sun, and W. Kong, "Efficiency optimization of PMSM drives using field-circuit coupled FEM for EV/HEV applications," *IEEE Access*, vol. 6, pp. 15192–15201, Mar. 2018.
[29] W. Chen, X. Zhang, X. Gu, Y. Yan, and T. Shi, "Band-based multi-step predictive torque control strategy for PMSM drives," *IEEE Access*, vol. 7, pp. 171411–171422, Nov. 2019.
[30] W. Liang, P. C.-K. Luk, and W. Fei, "Investigation of magnetic field interharmonics and sideband vibration in the FSCW IPMSM drive with the SPWM technique," *IEEE Trans. Power Electron.*, vol. 33, no. 4, pp. 3315–3324, Apr. 2018.
[31] H.-Y.-O. Yang and R. D. Lorenz, "Torque ripple minimization in six-step PMSM drives via variable and fast DC bus dynamics," *IEEE Trans. Ind. Appl.*, vol. 55, no. 4, pp. 3791–3802, Jul. 2019.
[32] V. Rallabandi, N. Taran, D. M. Ionel, and P. Zhou, "Inductance testing for IPM synchronous machines according to the new IEEE std 1812 and typical laboratory practices," *IEEE Trans. Ind. Appl.*, vol. 55, no. 3, pp. 2649–2659, May 2019.

SEONWOO JEON received the B.S. and M.S. degrees in electrical engineering from Yeungnam University, Gyeongsan, South Korea, in 2014 and 2016, respectively. He is currently pursuing the Ph.D. degree with the Department of Electrical Engineering, Hanyang University, Seoul, South Korea. His current research interests include a battery management systems and a power conversion system for EVs/HEVs.

GANG SEOK LEE received the B.S. degree in electrical and control engineering and the M.S. degree in electrical engineering from Hanyang University, Seoul, South Korea, in 2013 and 2015, respectively, where he is currently pursuing the Ph.D. degree with the Department of Electrical Engineering. His research interests include design, analysis, and testing and control of motor/generator and power conversion systems.

DONG-WOO KANG (Member, IEEE) received the B.S., M.S., and Ph.D. degrees in electrical engineering from Hanyang University, Seoul, South Korea, in 2006, 2008, and 2011, respectively. In 2014, he worked at Siemens AG A&D and Samsung Electronics. Since 2014, he has been a Professor with the Department of Electrical Energy Engineering, Keimyung University. His research interests include design, analysis of electric machines, power conversion systems for applications of vehicle, automotive parts, and robotics and industry operation systems.

WON-HO KIM received the B.S., M.S., and Ph.D. degrees in electrical engineering from Hanyang University, Seoul, South Korea, in 2005, 2007, and 2011, respectively.

From 2011 to 2017, he was a Research Staff Member with the Samsung Advanced Institute of Technology, Yongin, South Korea. Since 2017, he has been an Assistant Professor with the Department of Electrical Engineering, Gachon University, Seongnam, South Korea. His research interests include design and analysis of motors and generators and their applications to vehicles, home appliances, and industrial electrical machinery.

SUNGWOO BAE (Member, IEEE) received the B.S. degree from Hanyang University, Seoul, South Korea, and the M.S.E. and Ph.D. degrees from the University of Texas, Austin, USA, all in electrical engineering, in 2006, 2009, and 2011, respectively. From 2012 to 2013, he was a Senior Research Engineer with the Power Center, Samsung Advanced Institute of Technology. From 2013 to 2017, he was with Yeungnam University. Since 2017, he has been an Associate Professor with the Department of Electrical Engineering, Hanyang University. In 2005, he was awarded the Grand Prize at the National Electrical Engineering Design Contest by the Minister of Commerce, Industry and Energy of the Republic of Korea.